Polymer 51 (2010) 430–436

Contents lists available at ScienceDirect

Polymer

journal homepage: www.elsevier.com/locate/polymer

Polytriazole/clay nanocomposites synthesized using in situ polymerization and click chemistry

Yun-Sheng Ye, Ying-Chieh Yen, Chih-Chia Cheng, Yu-Jyuan Syu, Yao-Jeng Huang, Feng-Chih Chang*

Institute of Applied Chemistry, National Chiao-Tung University, Hsin-Chu, Taiwan, ROC

ARTICLE INFO

Article history:
Received 25 August 2009
Received in revised form
5 November 2009
Accepted 9 November 2009
Available online 27 November 2009

Keywords:
Clay
In situ polymerization
Click chemistry

ABSTRACT

This manuscript describes the preparation of polytriazole/clay nanocomposites through in situ polymerization of PTA, using click chemistry, in the presence of a propargyl-modified clay. The clay layers became exfoliated and dispersed well in the PTA matrix, thereby improving the thermal and mechanical properties of the clay. This approach can be extended to combine propargyl-modified clays with other azide- and alkyne-containing polymers.

1. Introduction

One of the most effective click reactions at present is the Huisgen 1,3-dipolar cycloaddition reaction of azides and terminal alkynes catalyzed by copper(I) complexes. This regioselective transformation proceeds with short reaction times, a wide range of tolerated functionality, high yields, and tolerance of humidity and oxygen [1–3]. As a result, this reaction has been applied extensively to various fields of materials science and polymer chemistry, such as branched dendrimers [5,6], surface modification [4,7–9], macromolecular engineering [10–14], nanostructured semiconductors [15] and polymer/clay nanocomposites [16,17]. The elaboration of linear polytriazoles (PTAs) through catalyzed and non-catalyzed click step growth polymerizations of dialkyne and diazide monomers, oligomers, and polymers has been investigated thoroughly [18–21]. Because PTAs are 1,2,3-triazole resins, they are thermally and thermo-oxidatively stable polymers—important characteristics for their application as macromolecules [22,23].

Polymer/clay nanocomposites have attracted great interest because of their engineering properties are often superior to those of the corresponding neat polymers [24–26]. Several approaches have been developed for the preparation of polymer-layered silicate nanocomposites, including solution exfoliation, melt intercalation, and in situ polymerization [27]. The most important challenge, however, when fabricating polymer/clay nanocomposites is how to achieve effective clay dispersion in the polymer matrix. In general, exfoliated structures are more effective at improving properties of the polymer (e.g., flame resistance and barrier, mechanical, electronic, and optical properties) than are intercalated structures because exfoliated nanostructures exhibit stronger synergistic effects of the polymer matrix and silicate layers. In situ polymerization appears to be a promising method for the preparation of exfoliated nanocomposites [16,28–36].

In this paper, we report that PTA/clay nanocomposites (e.g., PTA 1, Scheme 1) possess dramatically improved thermal (T_g = 123.5 °C; T_{d10} = 348.7 °C; CTE = 215.5 μm/m °C) and mechanical properties (max. stress = 34.9 MPa) relative to those of the neat PTA (T_g = 104.5 °C; T_{d10} = 337.6 °C; CTE = 337.9 μm/m °C; max. stress = 24.2 MPa). We prepared a propargyl-functionalized clay and reacted it with azides and alkynes to form PTA polymers through click reactions. In principle, this approach can be extended to the reactions of other propargyl-modified clays with other azide- and alkyne-containing polymers.

2. Experimental section

2.1. Materials

Ethanol (≥99.5%, Aldrich), HCl (37%, Sigma–Aldrich), acetic anhydride (≥99%, Sigma–Aldrich), sodium hydroxide (≥97.0%, Sigma–Aldrich), sodium azide (≥99.0%, Sigma–Aldrich), tetrabutylammonium bromide (99%, Aldrich), bromoundecanoic acid (99%, Aldrich), anhydrous magnesium sulfate (99%, Sigma–Aldrich),

* Corresponding author. Tel.: +886 3 5727077; fax: +886 3 5719507.
E-mail address: changfc@mail.nctu.edu.tw (F.-C. Chang).

0032-3861/$ – see front matter © 2009 Elsevier Ltd. All rights reserved.
doi:10.1016/j.polymer.2009.11.015

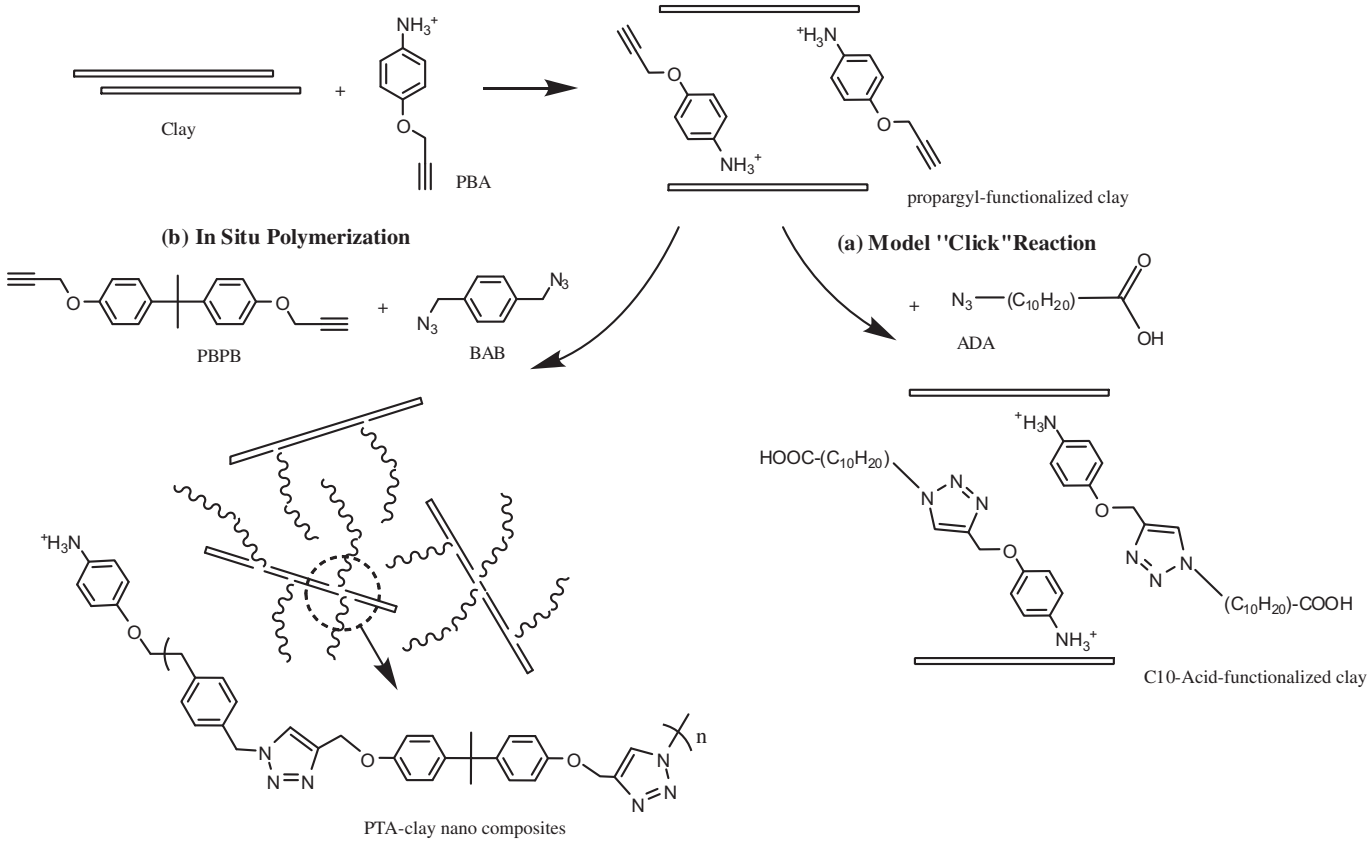

Scheme 1. Propargyl-functionalized clay and its click reactions with ADA (a, mode click reaction) and PBPB and BAB (b, in situ polymerization).

p-aminophenol (99%, Acros Organics), copper(I) iodide (≥97%, Riedel–de Haën), and sodium montmorillonite (Na^+-MMT; cationic exchange capacity: 1.45 meq/g; Nanocor Co) were used as received. *p*-Xylylene dichloride (≥98.0%, Sigma–Aldrich) was recrystallized from MeOH prior to use. Propargyl bromide (ca. 80 vol% in toluene, Fluka) was distilled prior to use.

2.2. Preparation of monomers

2.2.1. N-(4-Hydroxphenyl)acetamide

Acetic anhydride (12.3 g, 120 mmol) was added to a stirred solution of *p*-aminophenol (10.9 g, 100 mmol) in water (40 mL) and then the suspension was stirred at 60 °C until a clear solution was obtained. After cooling to ambient temperature, the precipitate was filtered off, washed with deionized water, and then recrystallized from water (79%). M.p. = 168 °C; ^{1}H NMR ($CDCl_3$): δ = 2.00 (e), 6.73 (b), 7.39 (c), 9.18 (a), 9.64 (d) ppm (Figure S1); ^{13}C NMR ($CDCl_3$): δ = 24.53 (6), 115.86 (2), 122.0 (3), 131.78 (4), 153.80 (1), 168.51 (5) ppm (Figure S2).

2.2.2. N-[4-(Prop-2-ynyloxy)phenyl]acetamide

N-(4-Hydroxyphenyl)acetamide (9.7 g, 60 mmol), NaOH (3.2 g, 80 mmol), deionized water 100 mL and tetrabutylammonium bromide (1.9 g, 6.0 mmol) were added into a three-necked round-bottom flask equipped with a magnetic stirrer, a reflux condenser, and a N_2 gas inlet tube and then the system was heated to 70 °C. Propargyl bromide (9.5 g, 80 mmol) was added dropwise over 3 h and then the mixture was maintained at 70 °C for 10 h. The reaction product was washed several times with deionized water to remove tetrabutylammonium bromide and the salts formed in the reaction. The product was recrystallized from EtOH (87%). M.p. = 122 °C; ^{1}H NMR (DMSO-d_6): δ = 2.00 (f), 3.51 (a), 4.74 (b), 6.89 (c), 7.49 (d), 9.80 (e) ppm (Figure S3); ^{13}C NMR (DMSO-d_6): δ = 24.38 (9), 56.15 (3), 78.80 (1), 80.16 (2), 115.33 (5), 121.42 (6), 133.58 (7), 153.89 (4), 168.76 (8) ppm (Figure S4).

2.2.3. 4-(Prop-2-ynyloxy)benzenaminium (PBA)

HCl (36%, 70 mL) was added to a solution in *N*-[4-(prop-2-ynyloxy)phenyl]acetamide (8.5 g, 45 mmol) in EtOH (70 mL) and then the mixture was stirred at 60 °C for 3 h. After cooling to ambient temperature, the product was filtered off and washed with EtOAc to give PBA as a brown solid (69%). M.p. = 50 °C; ^{1}H NMR (DMSO-d_6): δ = 3.57 (a), 4.78 (b), 7.05 (c), 7.32 (d), 10.37 (e) ppm (Figure S5); ^{13}C NMR (DMSO-d_6): δ = 56.40 (3), 79.0 (1,2), 116.44 (5,6), 80.16 (2), 125.04 (7), 157.01 (6) ppm (Figure S6).

2.2.4. 4,4′-(Propane-2,2-diyl)bis[(prop-2-ynyloxy)benzene] (PBPB)

PBPB was synthesized (89%) using a procedure similar to that described above [N-(4-Hydroxphenyl)acetamide replaced by bisphenol A]; its purification was performed using the same procedure used for *N*-[4-(prop-2-ynyloxy)phenyl]acetamide. M.p. = 78 °C; ^{1}H NMR ($CDCl_3$): δ = 1.68 (e), 2.53 (a), 4.68 (b), 6.89 (c), 7.17 (d) ppm (Figure S7); ^{13}C NMR ($CDCl_3$): δ = 31.54 (9), 42.26 (8), 55.99 (3), 75.68 (1), 79.25 (2), 114.47 (5), 128.20 (6), 144.37 (7), 155.61 (4) ppm (Figure S8).

2.2.5. 1,4-Bis(azidomethyl)benzene (BAB)

p-Xylylene dichloride (8.8 g, 50 mmol), NaN_3 (9.75 g, 150 mmol), DMF (100 mL), and benzene (100 mL) were added into a three-necked round-bottom flask equipped with a magnetic stirrer and a reflux condenser. The reaction mixture was slowly heated to 80 °C and then maintained at that temperature for 12 h. It was then poured into a beaker containing deionized water (200 mL). The organic layer was separated and then the aqueous layer was extracted three times

with benzene. All combined organic phases were dried overnight ($MgSO_4$) and then the benzene was distilled off to yield a light-yellow solid (81%). M.p. = 27–29 °C; ^{1}H NMR ($CDCl_3$): $\delta = 4.32$ (b), 7.35 (a) ppm (Figure S9); ^{13}C NMR ($CDCl_3$): $\delta = 54.59$ (1), 128.98 (3), 135.97 (2) ppm (Figure S10).

2.2.6. 11-Azidoundecanoic acid (ADA)

NaN_3 (6.5 g, 100 mmol) was added to a solution of 11-bromoundecanoic acid (7.95 g, 30 mmol) in DMSO and then the clear colorless solution was stirred at room temperature overnight. The reaction mixture was diluted with water and then HCl was added cautiously. After cooling the reaction mixture, the aqueous phase was then extracted three times with EtOAc. The combined organic layers were washed three times with water and then with brine before drying ($MgSO_4$). After filtration, all volatiles were evaporated under reduced pressure to yield the crude product as pale yellow oil. Purification through flash column chromatography (hexane) gave the product as a waxy solid (75%). ^{1}H NMR ($CDCl_3$): $\delta = 1.26$ (d, e), 1.58 (c), 2.31 (b), 3.20 (f), 10.29 (a) ppm (Figure S11); ^{13}C NMR ($CDCl_3$): δ = 26.86 (3), 27.01 (7), 29.20 (4,5), 34.24 (2), 51.59 (6), 180.59 (1) ppm (Figure S12).

2.3. Modification of clay

The propargyl-functionality modified clay was prepared through cationic exchange between Na^+-MMT and the clay-modifying agent (PBA) in an aqueous solution. Na-MMT was dispersed in deionized water at 60 °C, and a separate solution of PBA in deionized water was heated and mixed at 60 °C for 24 h. The propargyl-functionality modified clay was recovered by filtration, followed by repeated washings of the filter cake with deionized water to remove the excess of ions. The final product was dried in a vacuum oven at room temperature for 24 h.

2.4. Model click reaction

The propargyl-modified clay (0.25 g), ADA (0.8 mL, 3.9 mmol), and DMF (10 mL) were placed in a round-bottom flask and stirred. A solution of CuI (5 mol%) in water (0.5 mL) was added to the mixture, which was heated overnight in an oil bath at 70 °C. The particles were recovered using the procedure described above.

2.5. Preparation of PTA/clay nanocomposites

The propargyl-functionalized modified clay (1, 3, or 5 wt% of the monomer) was mixed with the monomers PBPB and BAB and DMF in a three-necked flask and heated at 70 °C for 30 min. CuI (5.0 mol%) was added and the mixture was stirred for 4 h. The PTA-clay nanocomposites were obtained through precipitation; they were then dried at 50 °C under vacuum for 24 h ^{1}H NMR (DMSO-d_6): $\delta = 1.53$ (e), 5.03 (c), 5.51 (b), 6.85 (c), 7.08 (h), 7.33 (d,g), 8.23 (a) ppm (Figure S13); ^{13}C NMR (DMSO-d_6): $\delta = 31.25$ (1), 36.61 (11), 41.74 (12), 53.12 (6), 61.67 (7), 114.62 (8), 125.46 (4), 128.25 (3,3′), 128.88 (9), 136.84 (5), 143.70 (10), 156.78 (7) ppm (Figure S14).

2.6. Characterization

FTIR spectra were recorded on a Nicolet Avatar 320 FTIR spectrophotometer over the range 4000–400 cm^{-1} at a resolution of 1.0 cm^{-1} under a continuous flow of N_2. ^{1}H NMR spectra were recorded at 25 °C on an INOVA 500 MHz NMR spectrometer. A DuPont Q100 thermogravimetric analyzer (TGA) was used to investigate the thermal stability of the nanocomposites; the samples (ca. 10 mg) were heated from ambient temperature to 850 °C under a N_2 atmosphere at a heating rate of 20 °C/min. The glass transition temperature (T_g) was determined by using a TA2000 differential scanning calorimeter (DSC) operated from 0 to 120 °C at a heating rate of 10 °C/min. Molecular weights and molecular weight distributions were determined through gel permeation chromatography (GPC) using a Waters 510 HPLC equipped with a 410 Differential Refractometer, a refractive index (UV) detector, and three Ultrastyragel columns (100, 500, and 103 A°) connected in series in order of increasing pore size. The polymer solution was purified by filtration through a 0.2-μm syringe filter before the GPC measurement. The coefficients of thermal expansion (CTEs) were obtained using a TA 2940 thermomechanical analyzer (TMA); the applied force applied was 0.005 N and the sample was heated from 25 to 120 °C at a rate of 5 °C/min. The morphology of the clay in the hybrids was observed using a JEOL JEM-1200CX-II transmission electron microscope operated at 120 kV. Wide-angle X-ray diffraction (WAXD) spectra were recorded for powdered samples using a Rigaku D/max-2500 type X-ray diffraction instrument. The tensile properties were measured according to ASTM 638 on a Shimadzu AG-50kNE universal tester. The crosshead speed was set at 1 mm/min.

3. Results and discussion

3.1. Characterization of propargyl-functionalized modified clay

Scheme 1 summarizes the various stages during the in situ intercalative polymerization of PTA using MMT nanoclays. In the first stage, the silica layers of the clay were modified with propargyl-functionality through ion exchange. In the XRD pattern in Fig. 1(b), the pristine MMT exhibits a basal spacing of 1.27 nm at a value of 2θ of 6.98°. This signal shifted slightly to 6.28° after the pristine clay had been modified with PBA, suggesting interlayer expansion. In the FTIR spectrum of pristine MMT [Fig. 1(a)], the band at 3628 cm^{-1} is typical of smectities, resulting from the internal OH groups of the clay minerals. We assign the signal at 1647 cm^{-1} to the water deformation band. After modification with propargyl-functionality, a characteristic propargyl signal appears near 3288 cm^{-1}. Moreover, the XRD pattern in Fig. 1(b) reveals that the peak at a value of 2θ of 6.98° shifted to 6.51° after modification. These FTIR spectra and XRD patterns provide evidence for the successful preparation of the propargyl-functionalized clay.

To confirm that clay layers could undergo click chemistry, we performed a model reaction between the propargyl-functionalized clay and the azide groups of ADA. The characteristic propargyl signal at 3288 cm^{-1} disappeared and a new signal appeared near 1740 cm^{-1}, corresponding to the carbonyl group of ADA [Fig. 1(a)]. Moreover, the XRD pattern in Fig. 1(b) reveals that the peak at an initial value of 2θ of 6.51° shifted to 5.58° after the click reaction. These results indicate that the azide-functionalized ADA had become attached to the clay layer—in particular, onto the surface of the interlayer of the silicate—through click chemistry.

3.2. Synthesis and characterization of PTA/clay nanocomposites

We mixed the propargyl-functionalized modified clay with the BAB and PBPB monomers to undergo polymerization to produce a series of PTA-clay composites (Scheme 1). Table 1 shows the intrinsic viscosity, molecular weights (M_w) and polydispersity indices (PDIs) of the PTA and its composites. The addition of clay resulted in a slight increase in the intrinsic viscosity and M_w. It is attributed to that MMT might either act as a catalytic agent or inactivates polymerization; resulting in a higher molecular weight of the PTA with proceeding polymerization [37]. This is also resulted in a slight decrease of PDI as clay loading was increased [38,39]. The efficiency of the click polymerization was clearly evident through ^{1}H NMR spectroscopic analysis (Fig. 2). The formation of triazole units

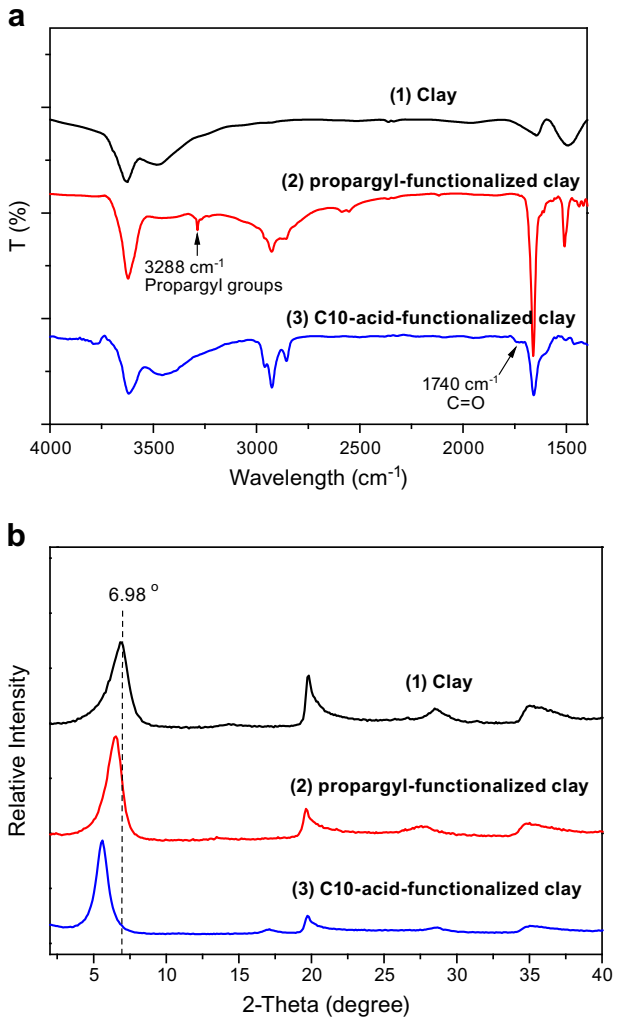

Fig. 1. (a) FTIR spectra of (1) the clay, (2) the propargyl-functionalized clay, and (3) the C10-acid-functionalized clay. (b) X-ray diffraction curves of (1) the clay, (2) the propargyl-functionalized clay, and the (3) C10-acid-functionalized clay.

was evidenced through the appearance of a signal at 8.21 ppm and shifts of the signals of the methylene protons adjacent to the alkyne (4.71 ppm) and azide (4.33 ppm) units to 5.57 and 5.06 ppm, respectively. Moreover, the broad signals in the spectrum of the polymer reveal that a high molar mass PTA/clay composite had formed.

3.3. Morphology of the PTA/clay nanocomposites

Fig. 3 displays XRD patterns of the pristine MMT, neat PTA, and a series of PTA-clay composites incorporating various clay contents.

Table 1
Polymerization of PTA in the presence of various amounts of clay.

Sample	Theoretical clay loading (wt%)[a]	Intrinsic viscosity ($dL\,g^{-1}$)[b]	M_w ($\times 10^6$)	M_w/M_n
PTA	0	0.63	5.54	2.98
PTA 1	1	0.69	5.89	2.75
PTA 3	3	0.73	5.95	2.49
PTA 5	5	0.71	6.12	2.58

[a] Determined from the initial clay loading and the mass of the monomer used.
[b] Determined at 25 °C.

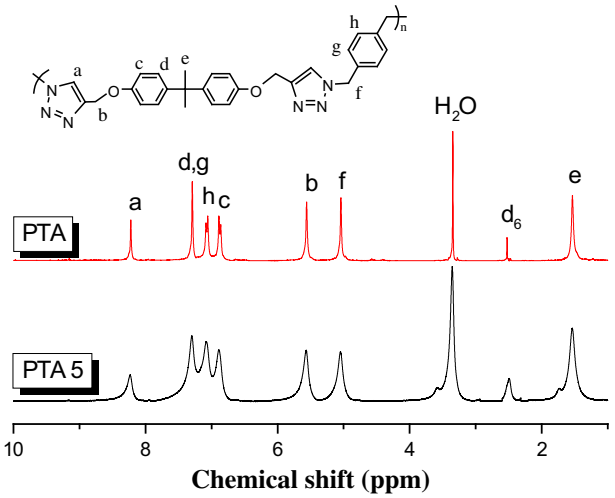

Fig. 2. ^{1}H NMR spectra of PTA and PTA 5.

For the PTA 1 nanocomposite, the d_{001} signal of the pristine MMT had disappeared completely, indicating the formation of an exfoliated structure in the nanocomposite. Moreover, upon incorporating 1 wt% of clay, the amorphous peak of the neat PTA ($2\theta = 20.23°$) shifted to a slightly lower value and a new amorphous peak appeared at a value of 2θ of 30.81°. A high distribution of clay plates in the PTA matrix tends to expand the intermolecular main chain spacing and reduce the intramolecular distance between the rigid polymer backbones [40–43]. PTAs 3 and 5 exhibited small and broad peaks having d-spacings of 1.48 and 1.67 nm, indicating that both exfoliated and intercalated structures were present. The intensity of the intercalated peak increased upon increasing the concentration of the clay, suggesting a higher fraction of intercalated clay [44].

To further investigate the dispersion of the clay in the polymer matrix, we recorded TEM micrographs, In Fig. 4, the dark lines represent clay layers; the bright areas, the PTA matrix. The XRD spectrum of PTA 1 exhibited only the broad peak of PTA matrix; its TEM micrographs [Fig. 4(a) and (d)] reveal that most of the clay layers lost their stacking structure and disorderly dispersed in the PTA

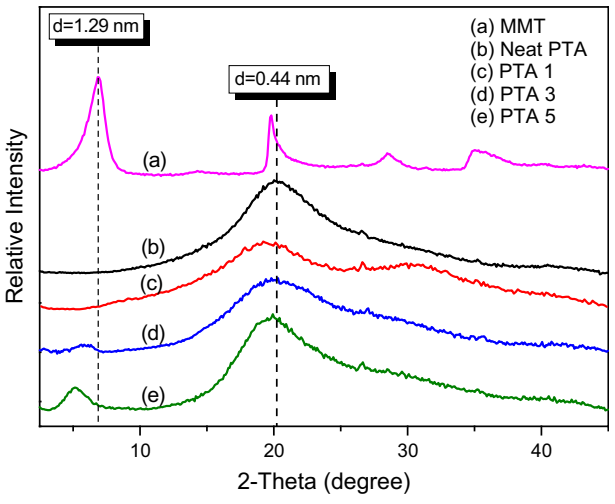

Fig. 3. Wide-angle X-ray diffraction patterns of the neat PTA and PTA-clay nanocomposites incorporating various clay contents.

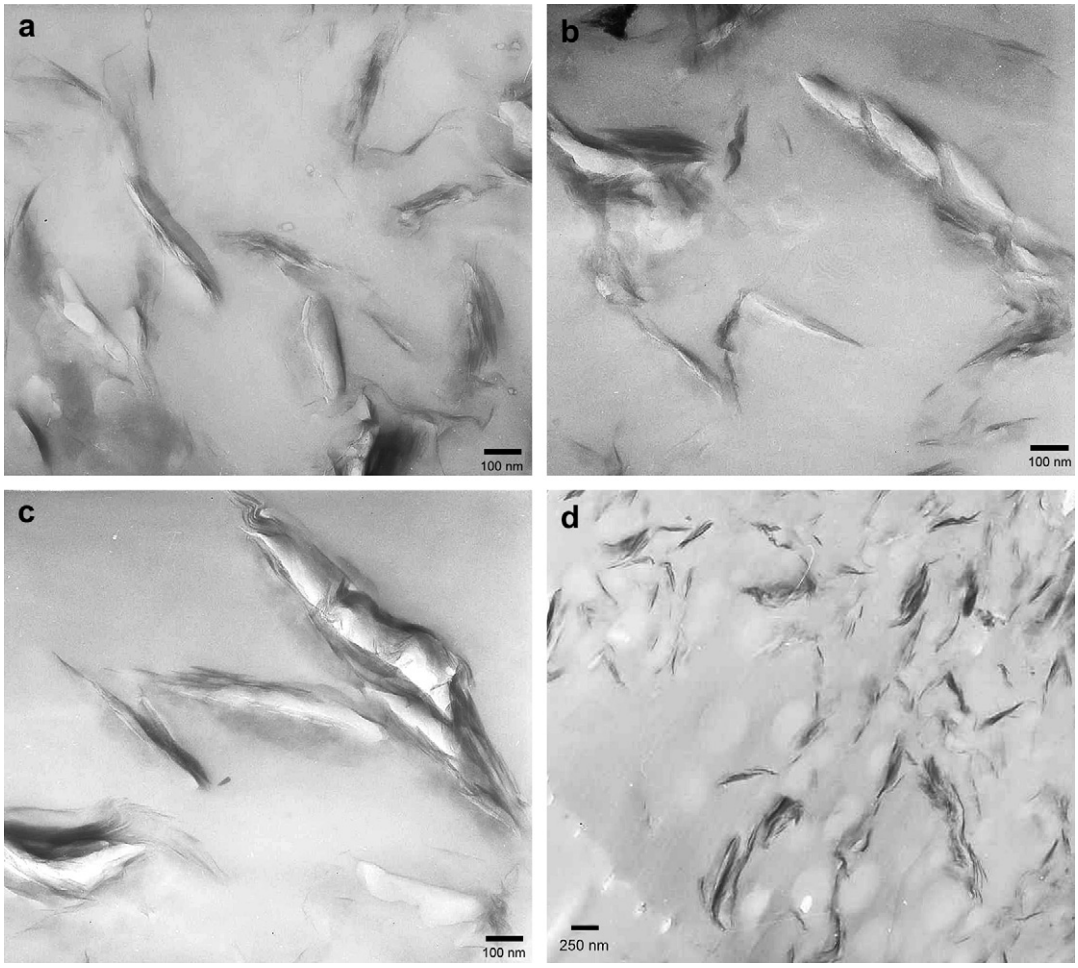

Fig. 4. TEM images of the (a) PTA 1 (80k), (b) PTA 3 (80k), (c) PTA 5 (80k), and (d) PTA 1 (10k) nanocomposites.

matrix. As the clay loading increased, certain degrees of aggregation led to the formation of intercalated stacks, as observed in Fig. 4(b) and (c). The TEM images in Fig. 4(a) and (b) clearly reveal that the exfoliated and intercalated structures coexisted in the PTA matrix.

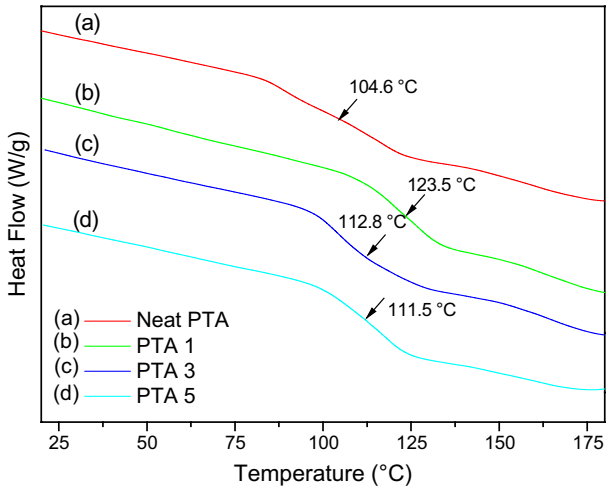

Fig. 5. DSC thermograms of the neat PTA and PTA-clay nanocomposites incorporating various clay contents.

3.4. Thermal and mechanical properties of PTA-clay nanocomposites

Fig. 5 and Table 2 summarize the glass transition temperatures (T_g) of the PTA-clay nanocomposites obtained from DSC measurements. All of the PTA-clay nanocomposites exhibited higher values of T_g than that of the neat PTA, due to restriction of the PTA chain motion. The fully exfoliated PTA 1 possessed a higher value of T_g relative to those of the partially exfoliated or intercalated composites (PTAs 3 and 5). An excessive level of clay plates above the saturation content tended to result in aggregation, thereby reducing the content of exfoliated clay in the PTA matrix. As a result, the ability to restrict chain motion was reduced, resulting in lower values of T_g (PTA 1 > PTA 3 > PTA 5).

Fig. 6 displays TGA thermograms of the PTA/clay nanocomposites; Table 2 summarizes the data. The values of T_{d10} of the PTA/clay

Table 2
Thermal and mechanical properties of PTA-clay nanocomposites.

Sample	T_g (°C)[a]	T_{d10} (°C)	T_{d60} (°C)	CTE (μm/m°C) 30–100 °C	Tensile strength (MPa)	Tensile modulus (GPa)	Elongation at break (%)
PTA	104.5	337.6	386.1	337.9	24.2	3.95	6.01
PTA 1	123.5	342.9	431.9	215.5	36.9	3.79	8.81
PTA 3	112.8	345.7	431.8	208.9	32.0	4.63	6.51
PTA 5	111.5	348.7	431.9	191.0	29.9	4.50	6.60

[a] Determined using DSC.

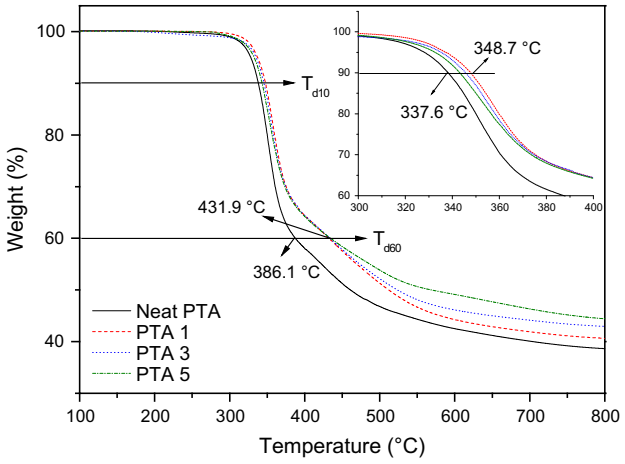

Fig. 6. TGA thermal degradation patterns of the neat PTA and PTA-clay nanocomposites incorporating various clay contents.

nanocomposites improved only slightly, whereas the value of T_{d60} showed a large increase, by 46 °C, relative to that of the neat PTA. We attribute the improvement in thermal stability of the PTA polymer filled with the nanoclay to the formation of a clay char that acted as a mass transport barrier and an isolator between the bulk polymer and the surface, where combustion occurred [44–47]. In addition, the restricted thermal motion of the polymer chains localized within the clay galleries also promoted the thermal stability of the polymer.

Table 2 reveals that the CTEs of the PTA/clay nanocomposites decreased upon increasing the clay content. We attribute the lower CTEs for the composites to the silicate rigidity and fine dispersion of the clay platelets in the PTA matrix. The incorporation of the modified clay reduced the CTEs and provided products exhibiting improved dimensional stability.

Fig. 7 presents the stress/strain curves for the elongation of the PTA/clay nanocomposites; again, Table 2 summarizes the data. The trend in the improved mechanical properties—namely, tensile strength and elongation-is identical to the data for the values of T_g; i.e., the exfoliated PTA 1 composite exhibited the greatest improvement. As mentioned above, when the clay content is alone, its saturation tends to reduce the concentration of the exfoliated clay in the PTA matrix and, thereby, decrease its ability to enhance the mechanical properties.

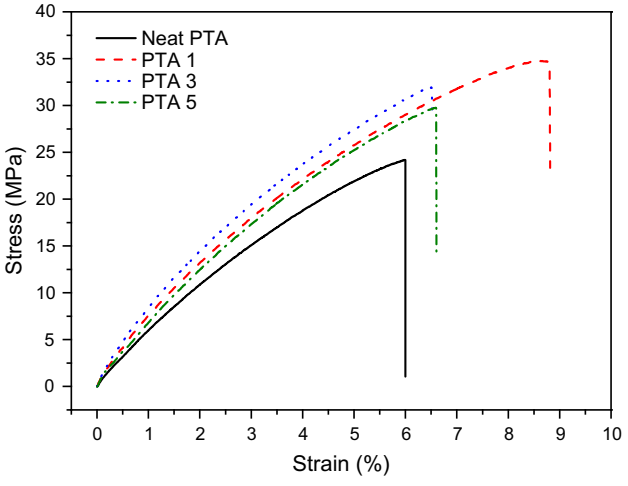

Fig. 7. Stress/strain curves for the neat PTA and PTA-clay nanocomposites incorporating various clay contents.

4. Conclusions

We have prepared PTA/clay nanocomposites through in situ polymerization of PTA using click chemistry in the presence of a propargyl-functionalized modified clay, as a new route toward high-performance PTA materials. The clay layers of PTA 1 were fully exfoliated and well dispersed in the PTA matrix, resulting in the greatest improvement in its thermal and mechanical properties. A clay content greater than the optimized saturation content caused these clay plates to aggregate (in the form of intercalation) and reduce the degree of exfoliation to below its saturation level within the PTA matrix; as a result, both the thermal and mechanical properties deteriorated.

Appendix. Supplementary data

Supplementary data associated with this article can be found in the online version, at doi:10.1016/j.polymer.2009.11.015.

References

[1] Kolb HC, Finn MG, Sharpless KB. Angew Chem Int Ed 2001;40:2004.
[2] Demko ZP, Sharpless KB. Angew Chem Int Ed 2002;41:2110.
[3] Rostovtsev VV, Green LG, Fokin VV, Sharpless KB. Angew Chem Int Ed 2002;41:2596.
[4] Evans RA. Aust J Chem 2007;60:384.
[5] Nugent A, Hawker C, Scheel A, Voit B, Pyun J, Fréchet JMJ, et al. Angew Chem Int Ed 2004;43:3928.
[6] Scheel AJ, Komber H, Voit BI. Macromol Rapid Commun 2004;25:1175.
[7] Fleming DA, Thode CJ, Williams ME. Chem Mater 2006;18:2327.
[8] Ranjan R, Brittain WJ. Macromolecules 2007;40:6217.
[9] Binder WH, Sachsenhofer R, Straif CJ, Zirbs R. J Mater Chem 2007;17:2125.
[10] Agut W, Tation D, Lecommandoux S. Macromolecules 2007;40:5653.
[11] Hawker CJ, Wooley KL. Science 2005;309:1200.
[12] Lutz JF. Angew Chem Int Ed 2007;46:1018.
[13] Opsteen JA, van Hest JCM. Chem Commun 2005:57.
[14] Ergin M, Kiskan B, Gacal B, Yagci Y. Macromolecules 2007;40:4724.
[15] Bakbak S, Leech PJ, Carson BE, Saxena S, King WP, Bunz UHF. Macromolecules 2006;39:6793.
[16] Tasdelen MA, Camp WV, Goethals E, Dubois P, Prez FD, Yagci Y. Macromolecules 2008;41:6035.
[17] Oral A, Tasdelen MA, Demirel AL, Yagci Y. Polymer 2009, doi:10.1016/j.polymer.2009.06.020.
[18] Binauld S, Damiron D, Hamaide T, Pascault JP, Fleury E, Drockenmuller E. Chem Commun 2008;35:4138.
[19] Diaz D, Punna S, Holze RP, McPherson AK, Sharpless KB, Fokin VV, et al. J Polym Sci Part A Polym Chem 2004;42:4392.
[20] Kiskan B, Demiray G, Yagci Y. J Polym Sci Part A Polym Chem 2008;46:3512.
[21] Liu XM, Thakur A, Wang D. Biomacromolecules 2007;8:2653.
[22] Xue L, Wan L, Hu Y, Shen X, Huang F, Lei D. Thermochim Acta 2006;448:147.
[23] Baut NL, Díaz DD, Punna S, Finn MG, Brown HR. Polymer 2007;48:239.
[24] Giannelis EP. Adv Mater 1996;8:29.
[25] Usuki A, Kawasumi M, Kojuma Y, Okada A, Kurauchi T, Kamigaito O. J Mater Res 1993;8:1174.
[26] Usuki A, Kamigaito O. J Mater Res 1993;8:1179.
[27] Alexandre M, Dubois P. Mater Sci Eng R 2000;28:63.
[28] Kubies D, Pantoustier N, Dubois P, Rulmont A, Jerome R. Macromolecules 2002;35:3318.
[29] Di JB, Sogah DY. Macromolecules 2006;39:5052.
[30] Zhao HY, Shipp DA. Chem Mater 2003;15:2693.
[31] Fu X, Qutubuddin S. Mater Lett 2000;42:12.
[32] Uthirakumar P, Song MK, Nah C, Lee YS. Eur Polym J 2005;41:211.
[33] Nese A, Sen S, Tasdelen MA, Nugay N, Yagci Y. Macromol Chem Phys 2006;207:820.
[34] Cui L, Tarte NH, Woo SI. Macromolecules 2008;41:4268.
[35] Tseng CR, Wu JY, Lee HY, Chang FC. J Appl Polym Sci 2002;85:1370.
[36] Fu HK, Huang CF, Huang JM, Chang FC. Polymer 2008;49:1305.
[37] Kim TH, Jang LW, Lee DC, Choi HJ, Jhon MS. Macromol Rapid Commun 2002;23:191.
[38] Biswas M, Ray SS. Polymer 1998;39:6423.
[39] Ballini R, Bigi F, Conforti ML, Santis DD, Maggi R, Oppici G, et al. Catal Today 2000;60:305.
[40] Tohnai N, Yoshiaki I, Miyata M, Yasui N, Eiko M, Kai Y. Bull Chem Soc Jpn 1999;72:851.

[41] Ye YS, Yen YC, Chen WY, Cheng CC, Chang FC. J Polym Sci Part A Polym Chem 2008;46:6296.
[42] Yen YC, Ye YS, Cheng CC, Chen HM, Sheu HS, Chang FC. Polymer 2008;49:3625.
[43] Cheng CC, Huang CF, Yen YC, Chang FC. J Polym Sci Part A Polym Chem 2008;46:6416.
[44] Delozier DM, Orwoll RA, Cahoon JF, Ladislaw JS, Smith JG, Connell JW. Polymer 2003;44:2231.
[45] Wang J, Du J, Zhu J, Wilkie CA. Polym Degrad Stab 2002;77:249.
[46] Wang GA, Wang CC, Chen CY. J Inorg Organomet Polymer 2005;15:3239.
[47] Zanetti M, Camino G, Reichert P, Mülhaupt R. Macromol Rapid Commun 2001;41:3218.